crystals

MDPI

Article

Floating Zone Growth of Sr Substituted Han Purple: $Ba_{0.9}Sr_{0.1}CuSi_2O_6$

Pascal Puphal [1,*], Stephan Allenspach [2,3], Christian Rüegg [2,3] and Ekaterina Pomjakushina [1,*]

1 Laboratory for Multiscale Materials Experiments, Paul Scherrer Institute, 5232 Villigen, Switzerland
2 Neutrons and Muons Research Division, Paul Scherrer Institute, 5232 Villigen, Switzerland; Stephan.Allenspach@psi.ch (S.A.); christian.rueegg@psi.ch (C.R.)
3 Department of Quantum Matter Physics, University of Geneva, 1205 Geneva, Switzerland
* Correspondence: pascal.puphal@psi.ch (P.P.); ekaterina.pomjakushina@psi.ch (E.P.)

Received: 16 April 2019; Accepted: 18 May 2019; Published: 27 May 2019

Abstract: We present a route to grow single crystals of $Ba_{0.9}Sr_{0.1}CuSi_2O_6$ suitable for inelastic neutron studies via the floating zone technique. Neutron single crystal diffraction was utilized to check their bulk quality and orientation. Finally, the high quality of the grown crystals was proven by X-ray diffraction and magnetic susceptibility.

Keywords: floating zone growth; seed crystal; low dimensional system; copper silicate; Han Purple

1. Introduction

Already in the Han Dynasty, the historically known compound Han Purple [1] $BaCuSi_2O_6$ was used as a purple coloring pigment in China. The rather blue compound [1] was possibly created in ancient times with a lot of Cu_2O (red) inside, thus mixing to a purple pigment. Han Purple can be found in nature, e.g., Africa, as the natural mineral Colinowensite [2]. Rediscovered and reported upon in 1989 [3], it attracted the interest of the physics community starting from 1997 [4], when the rare arrangement of the Cu ions as pairs on a two dimensional square lattice (see Figure 1) was noticed to form dimers with a singlet ground-state and triplet excited states. As the triplet state Zeeman split, in high magnetic fields, a two-dimensional Bose–Einstein condensate (BEC) of the bosonic triplet quasiparticles created a strong interest [5,6] in the compound. This interest was investigated after the discovery of an incommensurately modulated low temperature structure below 100 K [7–9] complicating the model and its physics. These studies were performed on $BaCuSi_2O_6$ crystals grown by two methods, namely, the floating zone (FZ) method in an oxygen flow [5,10] and from an oxygen spending lithiummetaborate flux [6,11], both with no detailed description of the growth conditions. Recently, we reported on the substitution series of (Ba,Sr)$CuSi_2O_6$, which stabilizes the tetragonal room temperature structure of $BaCuSi_2O_6$ down to lowest temperatures already with 5% substitution [12]. In a following study, we could show the growth conditions of $BaCuSi_2O_6$ single crystals and its Sr-substituted variant [13] by self melt growth in oxygen pressure. The resulting crystals have a typical size of $2 \times 1 \times 0.5\,mm^3$. Here we report on the floating zone growth of $Ba_{0.9}Sr_{0.1}CuSi_2O_6$, where large, high-quality single crystals are obtained for the first time, enabling future studies by, e.g., neutron spectroscopy.

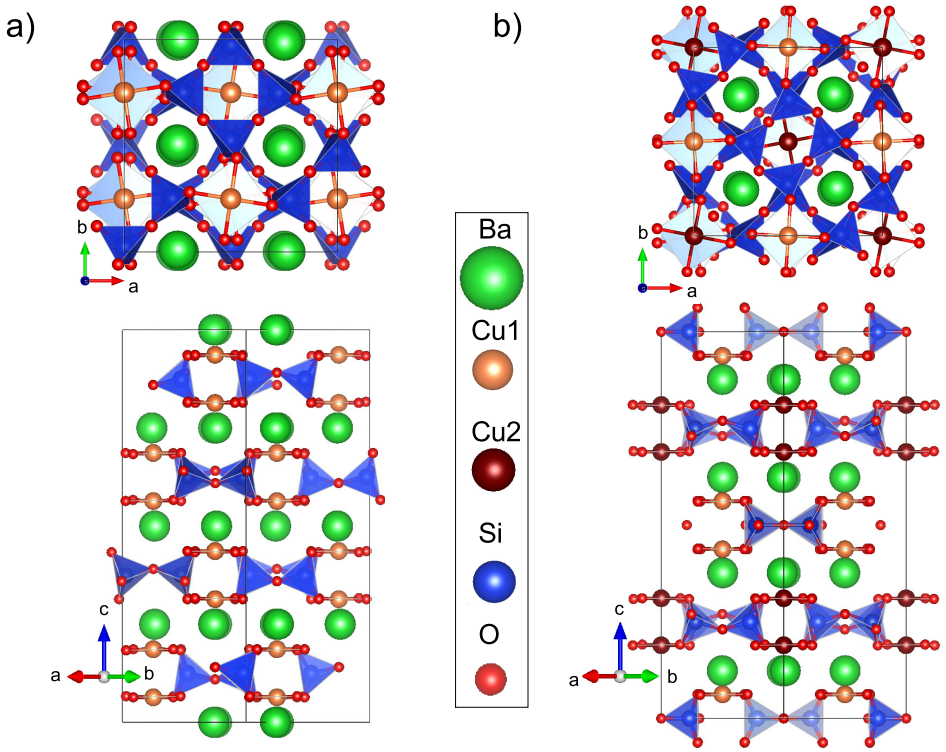

Figure 1. (**a**) Room temperature $I4_1/acd$ structure of Han Purple shown along the *c*-axis and the (1 1 0) direction [10]. (**b**) Same arrangement of the low temperature *Ibam* structure of Han Purple [8].

2. Experimental Details

Thermogravimetric analysis was performed using a NETZSCH STA 409 analyzer. The polycrystalline rods for the floating-zone growth were pressed in a Powloka hydrostatic press. The floating-zone growth was performed in a CSC FZ-1000-H-VI-VP-PC with a 300 W halogen lamp (FZ1) and a SCIDRE HKZ equipped with a 5 kW xenon lamp (FZ2). The powder X-ray diffraction measurement was performed using a Bruker D8 Advance with a Cu cathode. Fluorescence spectra were recorded using the Orbis microXRF analyzer from EDAX. Neutron diffraction experiments were carried out on the MORPHEUS two-axis diffractometer at SINQ (PSI) at room temperature using a wavelength of $\lambda = 5$ Å. Magnetic susceptibility measurements were carried out in a range of 1.8–300 K at 0.1 T using a quantum design physical property measurements system (PPMS). A laboratory X-ray Laue equipped with CCD camera (Photonic Science) was used to orient the samples.

3. Synthesis

Polycrystalline $Ba_{0.9}Sr_{0.1}CuSi_2O_6$ was prepared by sintering stoichiometric amounts of $BaCO_3$, $SrCO_3$, CuO, and SiO_2. The powder was ground and sintered in an aluminum oxide crucible in air at 1028 °C for 2 months, with several intermediate grindings to remove any early stage phases in the silicate formation [1] as $BaCu_2Si_2O_7$. Its phase purity was checked with laboratory X-ray diffraction, proving to be of the $I4_1/acd$ structure (s.g. 142) shown in Figure 1a. The powder was then pressed into rods of a 7 mm diameter by a hydrostatic press (∼4000 bar) using rubber forms and subsequently annealed for 24 h in air at 1030 °C. The rod density was checked via dilatometry and found to be above 92%. Finally, single crystals were grown using FZ1 as described below.

We performed differential scanning calorimetry (DSC), including a thermogravimetric (TG) analysis, on the growth conditions of $Ba_{0.9}Sr_{0.1}CuSi_2O_6$ and observed the reduction of Cu^{2+} to Cu^{1+} while releasing oxygen ($2CuO \longrightarrow Cu_2O + \frac{1}{2}O_2$) monitored by a mass loss in the TG signal, followed directly by the melting of the compound. Afterwards, the melting turns it to a viscous mass that glazes when cooled in air. However, upon applying oxygen pressure, the decomposition is shifted up further than the melting temperature seen in a DSC experiment performed in air compared to one in oxygen flow with a partial pressure of 1.3 bar [13] (see Figure 2). Using a linear interpolation, the difference between decomposition and melting would meet at around 2 bar. Thusm one would expect optimal growth conditions above this oxygen pressure.

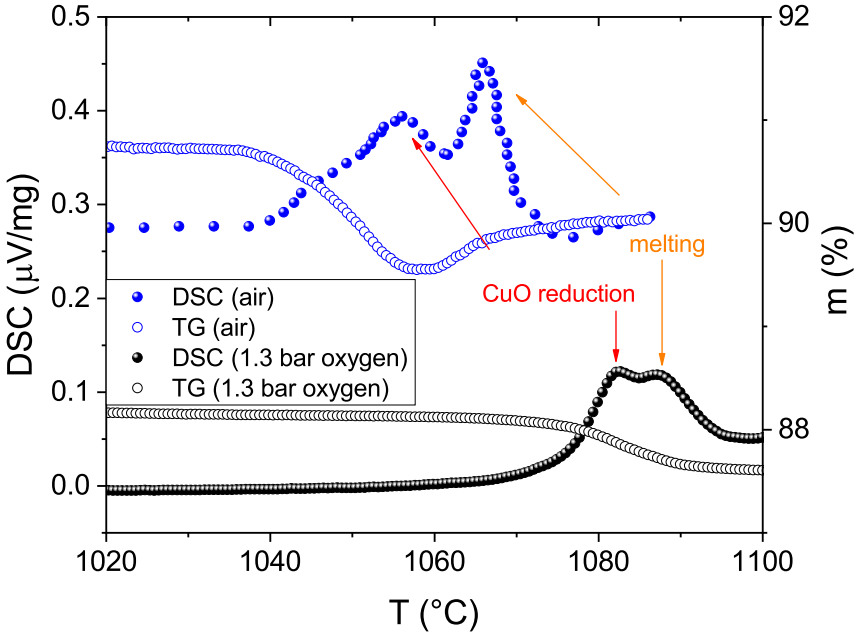

Figure 2. Differential scanning calorimetry/thermogravimetric (DSC/TG) measurement of a stoichiometric $BaCO_3$, CuO, and 2 SiO_2 mixture upon heating in air and an oxygen partial pressure of 1.3 bar.

To obtain large (cm^3-size) single crystals of $Ba_{0.9}Sr_{0.1}CuSi_2O_6$, we utilized the floating zone growth method using two furnaces equiped with halogen lamps (FZ1) and a xenon lamp (FZ2). As $BaCuSi_2O_6$ has a relative low melting point of around 1060 °C, which is slightly lowered by Sr substitution [12], a low-power halogen lamp (FZ1) with a better focus can be applied. As a first growth attempt, we followed the short report on the floating zone growth of $BaCuSi_2O_6$ from [5], and we used the same conditions for the substituted variant attempting a growth rate of 0.5 mm/h in an oxygen flow of 200 cc/min. Stoichiometric seed and feed rods with a diameter of 7 mm and a length of 7 cm were used. With these conditions, we were unable to obtain a stable growth, as the reduction of CuO to Cu_2O led to bubble formations in the liquid zone, causing the rods to disconnect (see Table 1 C1).

Table 1. Listed are the growth attempts of $Ba_{0.9}Sr_{0.1}CuSi_2O_6$ using stoichiometric seed and feed rods of 7 cm length and 7 mm diameter for FZ. Added as CF is the flux growth of Han Purple after [11].

	Furnace	Gas	p [bar]	Power [%]	Rate [mm/h]	Comments	Crystallite Size
C1	FZ1	O_2	0	53.7	-	could not start growth, immense bubbles	0
C2	FZ1	O_2	0.5–3	54–56.3	2-0.5	neck thinning and bubbles	µm
C3	FZ1	O_2	7	59	-	bubbles	0
C4	FZ2	O_2	30	16–18	1	flowing down of liquid, disconnection	0
C5	FZ2	O_2	100	22	2	repeated disconnection, phase seperation	0
C6	FZ1	O_2/Ar	4.4	56	1	stable growth conditions	mm
C7	FZ1	O_2/Ar	7	56.3	0.5	stable growth conditions	mm-cm
C8	FZ1	O_2/Ar	5.4	54.7	0.5	(seedcrystal) stable growth conditions	cm
CF	flux			--		2:1 $LiBO_2$, 1000 °C slow cooling to 875 °C	mm

3.1. Atmosphere

Surprisingly, an increase of pressure with attempts at 0.5, 1, 2.5, 3, 4, 5, and 7 bar led to similar problems and could not stabilize the melt and suppress the bubble formation (C2,3). In all cases, when changing the lamp power by a few percentage points, the melt was either too viscous at low lamp power or the temperature was too high, leading to a decomposition. This implies that the decomposition and melting point are still overlapping, as seen in the DSC curve. As CuO can only be grown at elevated oxygen pressures [14,15], we wanted to attempt even higher pressures to ensure a clear separation of the CuO reduction and melting point following an extrapolation of Figure 2. Even upon application of 100 bar of oxygen pressure (using FZ2), we were still unable to stabilize the liquid zone (C4). Repeated disconnection complicated the growth attempt, and afterwards, we could still find orange parts of reduced copper oxide on crushed pieces of the obtained crystal. Thus, in order to find stable growth conditions with FZ1, the experience of applying an oxygen–argon mixture in the comparable compound of $SrCu_2(BO_3)_2$ [16,17] was used. Varying the pressure and oxygen/argon mixture leads to a liquidification of the melt and a breaking of the bubbles into smaller, not visible, ones with increasing argon content, which stabilizes the growth conditions. We found that the concentration of argon has to exceed the oxygen one for this effect. Nevertheless, in a cross section of obtained multigrain crystals, there is still some orange Cu_2O phase present, proving the continuation of a decomposition at any attempted pressure and mixture of gases. Without the possibility of a full suppression of the CuO reduction, we studied the growth in stable conditions using four 300 W lamps operated at 54.5% with 5 bar pressure obtained with 0.4 L/min argon and 0.1 L/min oxygen gas-flow: Only in the case of several simultaneously growing grains is the Cu_2O impurity incorporated in between the grains, while with a single grain, the impurity is pushed up with the liquid zone until the very last part of the melt. Thus, the orange Cu_2O is kept in the molten zone without any influence on the single crystal formation.

3.2. Growth Speed

$Ba_{0.9}Sr_{0.1}CuSi_2O_6$ crystals grow quickly along the *a*-direction, while the *c*-direction develops much slower, leading to growth steps and, thus, faceted structures (terraces) of the crystal flakes grown by direct melt [13]. This leads to the a-axis developing as the growth direction in FZ experiments, while the *c*-axis points perpendicular to the round surface. With growth rates of 1 mm/h, several grains develop with a tilt in the *ab*-plane limited by the c-direction growth rate (C6). We thus reduced the growth rate to 0.5 mm/h (C7) and additionally started to grow with a single crystal as a seed (C8) oriented with the c axis pointing along the growth direction (see Figure 3a,b) to prevent the formation of the misaligned grains. The seed-crystal was glued to the seed-rod by GEvarnish and then molten to it with the optical furnace by quickly melting the tip of the seed-rod, where the organic glue is fully burned away. Then the growth was started by melting the feed only and moving seed and feed together. Meanwhile, the forced

growth orientation along the *c*-direction was not successful, as throughout the growth the growing crystal went back to the preferred orientation, the prevention of additional grains was successful in the entire grown crystal. Even with the chosen method of floating zone growth, the usually round crystal shows a shiny facet on both sides perpendicular to the *c* direction (see Figure 4d). In this case, as there was a reorientation, which was not completed after the end of the growth, there is an angle of 30° between the growth direction and the *a*-axis (see inset of Figure 5d).

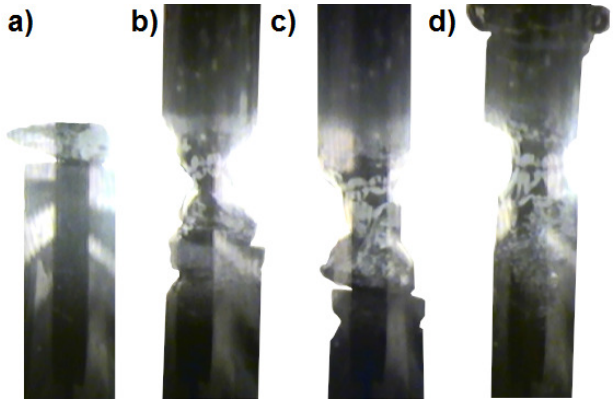

Figure 3. Images of the floating zone growth, with (**a**) showing the glued crystal seed on the top of the seed rod, (**b**) the start of the growth, and (**c**,**d**) the evolution after several hours of growing.

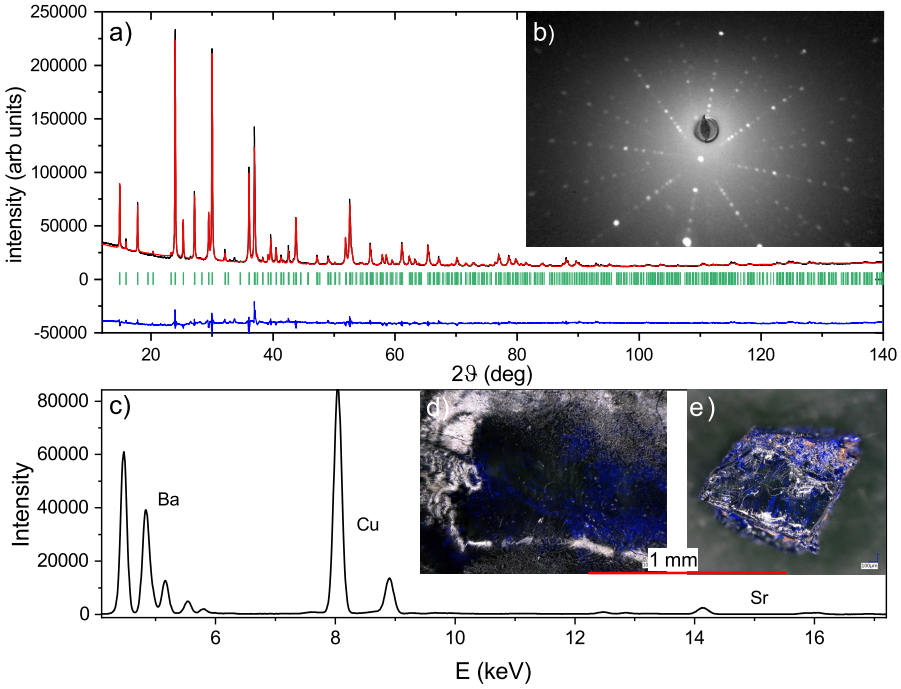

Figure 4. (**a**) Rietveld refinement of the crystal structure parameters of $Ba_{0.9}Sr_{0.1}CuSi_2O_6$ crushed single crystals, based on laboratory X-ray powder diffraction data at 295 K. The rows of ticks in the middle correspond to the calculated diffraction peak positions of the $I4_1/acd$ structure. (**b**) Laue image on the shiny side of the single crystal shown in Figure 5b revealing the *c*-axis of the tetragonal system. (**c**) MicroXRF spectra of the $Ba_{0.9}Sr_{0.1}CuSi_2O_6$ single crystal C8. (**d**) Magnified image of a section from the FZ crystal C8 (**e**) Broken piece of an FZ grown crystal solely in oxygen atmosphere C2.

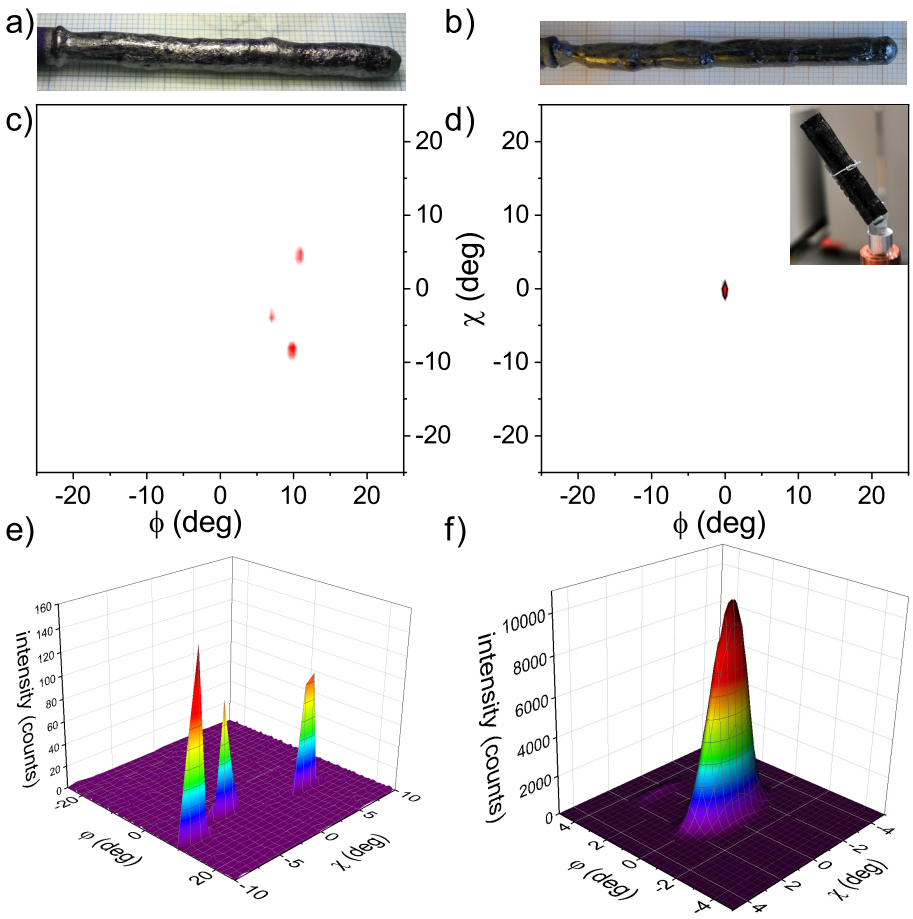

Figure 5. Comparison of crystal C6 grown with 1 mm/h (**a**,**c**,**e**) and C8 0.5 mm/h (**b**,**d**,**f**). Image of the floating zone grown crystal is given in (a,b) and then their neutron scattering scans of the (0 0 4) reflection plotted versus two rotation angles. First, a contour plot in (c,d) shows a larger area displaying the amount of grains and second, a 3D surface plot in (e,f) reveals the detailed shape.

4. Characterization

$Ba_{0.9}Sr_{0.1}CuSi_2O_6$ crystals cleave well perpendicular to the *c*-direction, leaving shiny *ab*-planes enabling an easy orientation when breaking off the last and first part of the growth. Obtained $Ba_{0.9}Sr_{0.1}CuSi_2O_6$ crystals were analyzed in a neutron scattering experiment using the MORPHEUS 2-axis diffractometer at SINQ (PSI) at room temperature with a wavelength of 5 Å (see Figure 5c–f). We scanned one reflection by fixing the detector to, e.g., $2\vartheta = 53.34°$ for the (0 0 4) reflection shown in Figure 5 and measured while rotating the crystal to search for additional grains. As discussed above, this neutron diffraction measurement revealed that earlier growth attempts with 1 mm/h gave rise to three grains developing rather equally throughout the rod. They are slightly tilted in the *ab*-plane in respect of each other but share a similar *c*-axis orientation perpendicular to the growth direction (see Figure 5c,e).

In the seeded 0.5 mm/h growth (C8), a full 180° rotation scan of the (0 0 4) reflection showed only one grain in the entire piece, giving a sizeable single crystal of several grams and 4 cm length (see inset of Figure 5d). We found a broadening of the reflection along one angle (see Figure 5f) due to the change of the growth direction along the crystal lenght.

We reproduced the flux growth for non ubstituted (as the flux reacts with Sr) Han Purple reported in [11] and compared the single crystal quality of both samples. All flux grown crystals as well as

crystals prepared with oxygen pressure in the way described in [13] and by the floating zone growth reported here can be obtained with equal quality (in the sense of magnetic impurities). In both ways, by direct melting with oxygen pressure and with flux, the magnetic impurity amount can range from 3 to 25%. The magnetic impurities can be analyzed in this system by fitting the Curie tail arising from free spin-1/2 levels (e.g., paramagnetic $BaCuSi_4O_{10}$) at low temperatures, which is entirely dominated by impurities. In Figure 6, we show a magnetic susceptibility measurement comparing high-quality crystals of $BaCuSi_2O_6$ grown with the flux technique to the $Ba_{0.9}Sr_{0.1}CuSi_2O_6$ single crystal grown with the floating zone technique. Both have a similar impurity amount of less than 1% magnetic impurities. The shift of the maximum, due to a smaller unit cell, for Sr substitution is apparent (see arrows in Figure 6). For the antiferromagnetic intradimer coupling parameter, a random phase approximation (RPA) fit yields $J_{float} = 45.9(1)$ K compared to $J_{flux} = 51.3(3)$ K. This hints at a full incorporation of 10% Sr following $J_{Sr} \approx (50 - 40x_{Sr})$ K, in agreement with the microXRF results of 9(2)% (see Figure 4c) and lattice constants of $a \approx 9.96206(9)$, $c \approx 22.2871(2)$ (obtained by the Rietveld refinement shown in Figure 4a), matching the published results from a powder sample [12]. The nonmagnetic Cu_2O can be observed optically as an orange impurity and changes the color from blue to purple. With its sharp contrast to blue, this impurity can be seen on cleaved surfaces in the microscope. In Figure 4d, we show first a magnification of the facet on the side of the floating zone crystal C8 and, second, a broken piece of an FZ growth attempt in oxygen pressure C2. In the second case, one can clearly see orange parts of reduced copper oxide, which is not present in the final growth. The Laue image in Figure 4b was taken on the surface of C8, i.e., Figure 4d, proving the *c*-direction orientation and crystal quality.

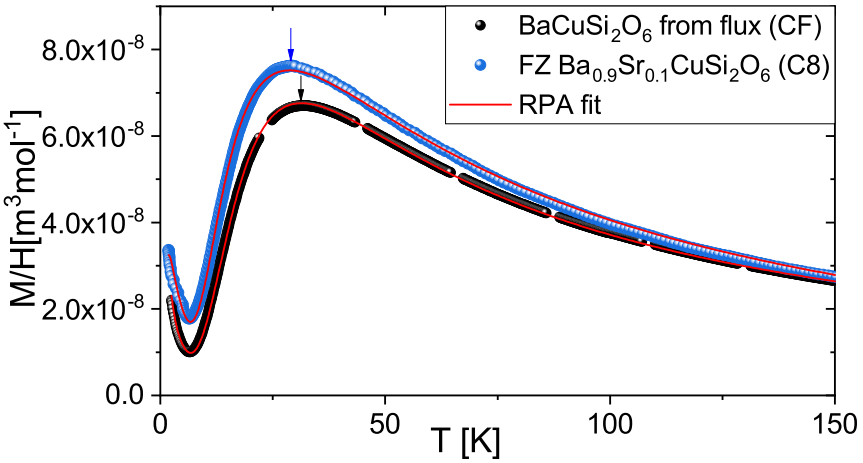

Figure 6. Temperature-dependent magnetic susceptibility of the two single crystals C8 and CF in the range of 1.8-300 K measured in a field of 0.1 T along the *a*-direction. A slight offset was chosen for visibility.

5. Summary

Via the optical floating zone growth of $Ba_{0.9}Sr_{0.1}CuSi_2O_6$, we obtained large single crystals suitable for further neutron studies. With an 80%–20% argon–oxygen mixture, stable conditions could be created at 5 bar of pressure. With these conditions, using four 300 W lamps at 54.5%, a single crystal is obtained, growing with a slow rate of 0.5 mm/h. The use of a seed crystal proved crucial to get a large single grain at this growth rate. By neutron single-crystal diffraction, we proved that a single grain is obtained, with the same crystal quality as flux grown $BaCuSi_2O_6$.

Author Contributions: Conceptualization, P.P., E.P.; methodology, P.P.; software, P.P., S.A.; validation, P.P., S.A.; formal analysis, P.P.; investigation, P.P., S.A.; resources, E.P.; data curation, P.P.; writing–original draft preparation, P.P.; writing–review and editing, P.P., C.R. and E.P.; visualization, P.P.; supervision, E.P, C.R..; project administration, E.P., C.R.; funding acquisition, E.P., C.R.

Funding: The authors would like to acknowledge the Swiss National Science Foundations (SNSF R'Equip, Grant No. 206021_163997 and Grant No. 206021_139082) and matching funds from Paul Scherrer Institute for purchasing the SCIDRE HKZ—high pressure high-temperature optical floating zone furnace and the MPMS.

Acknowledgments: This work is partly based on experiments performed at the Swiss spallation neutron source SINQ, Paul Scherrer Institute, Villigen, Switzerland. The measurements were carried out on the PPMS/MPMS devices of the Laboratory for Multiscale Materials Experiments, Paul Scherrer Institute, Villigen, Switzerland.

Conflicts of Interest: The authors declare no conflict of interest.

References

1. Berke, H. The invention of blue and purple pigments in ancient times. *Chem. Soc. Rev.* **2007**, *36*, 15–30. [CrossRef] [PubMed]
2. Rieck, B.; Pristacz, H.; Giester, G. Colinowensite, $BaCuSi_2O_6$, a new mineral from the Kalahari Manganese Field, South Africa and new data on wesselsite, $SrCuSi_4O_{10}$. *Mineral. Mag.* **2015**, *79*, 1769–1778. [CrossRef]
3. Finger, L.W.; Hazen, R.M.; Hemley, R.J. $BaCuSi_2O_6$: A new cyclosilicate with four-membered tetrahedral rings. *Am. Mineral.* **1989**, *74*, 952–955.
4. Sasago, Y.; Uchinokura, K.; Zheludev, A.; Shirane, G. Temperature-dependent spin gap and singlet ground state in$BaCuSi_2O_6$. *Phys. Rev. B* **1997**, *55*, 8357–8360. [CrossRef]
5. Jaime, M.; Correa, V.F.; Harrison, N.; Batista, C.D.; Kawashima, N.; Kazuma, Y.; Jorge, G.A.; Stern, R.; Heinmaa, I.; Zvyagin, S.A.; et al. Magnetic-Field-Induced Condensation of Triplons in Han Purple Pigment$BaCuSi_2O_6$. *Phys. Rev. Lett.* **2004**, *93*, 087203. [CrossRef] [PubMed]
6. Sebastian, S.E.; Harrison, N.; Batista, C.D.; Balicas, L.; Jaime, M.; Sharma, P.A.; Kawashima, N.; Fisher, I.R. Dimensional reduction at a quantum critical point. *Nature* **2006**, *441*, 617–620. [CrossRef] [PubMed]
7. Rüegg, C.; McMorrow, D.F.; Normand, B.; Rønnow, H.M.; Sebastian, S.E.; Fisher, I.R.; Batista, C.D.; Gvasaliya, S.N.; Niedermayer, C.; Stahn, J. Multiple Magnon Modes and Consequences for the Bose-Einstein Condensed Phase in$BaCuSi_2O_6$. *Phys. Rev. Lett.* **2007**, *98*, 017202. [CrossRef] [PubMed]
8. Sheptyakov, D.V.; Pomjakushin, V.Y.; Stern, R.; Heinmaa, I.; Nakamura, H.; Kimura, T. Two types of adjacent dimer layers in the low-temperature phase of $BaCuSi_2O_6$. *Phys. Rev. B* **2012**, *86*, 014433. [CrossRef]
9. Samulon, E.C.; Islam, Z.; Sebastian, S.E.; Brooks, P.B.; McCourt, M.K.; Ilavsky, J.; Fisher, I.R. Low-temperature structural phase transition and incommensurate lattice modulation in the spin-gap compound$BaCuSi_2O_6$. *Phys. Rev. B* **2006**, *73*, 100407. [CrossRef]
10. Sparta, K.M.; Roth, G. Reinvestigation of the structure of $BaCuSi_2O_6$—Evidence for a phase transition at high temperature. *Acta Crystallogr. Sect. B Struct. Sci.* **2004**, *60*, 491–495. [CrossRef] [PubMed]
11. Sebastian, S.E.; Tanedo, P.; Goddard, P.A.; Lee, S.C.; Wilson, A.; Kim, S.; Cox, S.; McDonald, R.D.; Hill, S.; Harrison, N.; Batista, C.D.; Fisher, I.R. Role of anisotropy in the spin-dimer compound$BaCuSi_2O_6$. *Phys. Rev. B* **2006**, *74*, 180401. [CrossRef]
12. Puphal, P.; Sheptyakov, D.; van Well, N.; Postulka, L.; Heinmaa, I.; Ritter, F.; Assmus, W.; Wolf, B.; Lang, M.; Jeschke, H.O.; et al. Stabilization of the tetragonal structure in$(Ba1\text{-}xSrx)CuSi_2O_6$. *Phys. Rev. B* **2016**, *93*, 174121. [CrossRef]
13. van Well, N.; Puphal, P.; Wehinger, B.; Kubus, M.; Schefer, J.; Rüegg, C.; Ritter, F.; Krellner, C.; Assmus, W. Crystal Growth with Oxygen Partial Pressure of the BaCuSi2O6 and Ba1–xSrxCuSi2O6 Spin Dimer Compounds. *Cryst. Growth Des.* **2016**, *16*, 3416–3424. [CrossRef]
14. Prabhakaran, D.; Boothroyd, A. Single crystal growth of Zn-doped CuO by the floating-zone method. *J. Cryst. Growth* **2003**, *250*, 77–82. [CrossRef]
15. Ito, T.; Yamaguchi, H.; Okabe, K.; Masumi, T. Single-crystal growth and characterization of Cu_2O and CuO *J. Mater. Sci.* **1998**, *33*, 3555–3566. [CrossRef]

16. Zayed, M.; Rüegg, C.; Pomjakushina, E.; Stingaciu, M.; Conder, K.; Hanfland, M.; Merlini, M.; Rønnow, H. Temperature dependence of the pressure induced monoclinic distortion in the spin Shastry–Sutherland compound $SrCu_2(BO_3)_2$. *Solid State Commun.* **2014**, *186*, 13–17. [CrossRef]
17. Dabkowska, H.; Dabkowski, A.; Luke, G.; Dunsiger, S.; Haravifard, S.; Cecchinel, M.; Gaulin, B. Crystal growth and magnetic behaviour of pure and doped $SrCu_2(11BO_3)_2$. *J. Cryst. Growth* **2007**, *306*, 123–128. [CrossRef]